# NHS Breast Screening Programme Equipment Report: Technical Evaluation of Hologic Envision digital mammography system in 2D mode

## February 2026

# Contents

Please note: The image shown in Figure 1 is courtesy of Hologic.

## Executive Summary

The technical performance of the Hologic Envision was assessed in 2D mode.

The Dance mean glandular dose (MGD) was found to be well below the remedial level for all automatic exposure control (AEC) dose modes. For a 53mm equivalent standard breast, the Dance MGD was 1.36mGy, compared with the remedial level of 2.5mGy. The image quality, measured by threshold gold thickness using the CDMAM 3.4 test object, was better than the NHSBSP ‘achievable level’.

Technical performance of this equipment operating in 2D mode was found to be satisfactory and the system could proceed to practical evaluation of 2D mode. The technical evaluation of the performance in tomosynthesis mode is published as a separate report.

## Background

Mammographic equipment approved for use in the NHSBSP is subject to evaluation commissioned by NHS England and carried out by a number of breast screening services in England who undertake the practical evaluation of equipment using protocols provided by the NHSBSP. These evaluations comprise a staged process as follows:

1. A technical evaluation by the National Coordinating Centre for the Physics of Mammography ("NCCPM") (the "Technical Evaluation")

2. If the Technical Evaluation meets requirements, a subsequent practical evaluation is conducted by one of the breast screening services involved in the NHSBSP (the "Practical Evaluation")

Technical and Practical Evaluations are undertaken to assess the use of equipment in a practical, clinical setting and are not intended to be clinical trials. Further information about the limitations of the Technical Evaluation and Practical Evaluations are set out below.

The purpose of the Technical and Practical Evaluations together are intended to:

- determine the suitability of the equipment for use within the NHSBSP
- assist potential purchasers in making their choice of equipment
- provide potential users with performance data about equipment
- provide potential users with a record of the practical experience of using the equipment in the NHSBSP
- enable comparisons to be made with other pieces of tested equipment.

## Disclaimer

Whilst NHS England commissions testing for the purposes outlined above, in order to provide further information and support to providers of screening services within the NHSBSP, it is for informational purposes only and such testing is subject to the limitations described below. No representation is made by NHS England in relation to the reports generated from the Technical Evaluation or the Practical Evaluation and, insofar as the law allows, NHS England accepts no liability arising from purchase or use of equipment by providers of screening services within the NHSBSP subjected to them.

Providers of screening services within the NHSBSP must ensure that all equipment purchased and used within the NHSBSP complies with all relevant requirements of the NHSBSP, the terms of their contracts in respect of the NHSBSP, and all other relevant obligations including but not limited to ensuring that such equipment:

- complies with national equipment standards
- has been approved for use in the programme and is tested by appropriately trained staff and medical physics services, in accordance with NHSBSP guidelines
- is accredited for use within the NHSBSP and that image quality and radiation dose meet acceptable standards
- is suitable for the usage intended in the breast screening unit.

Providers are reminded that they should carry out their own due diligence in respect of the above.

Testing undertaken during the Technical Evaluation is a balance between time, evaluation costs and depth. There are therefore limitations to the scope of the Evaluations undertaken on the behalf of the NHSBSP.

The Technical Evaluation is undertaken over a short time and so will not assess if image quality may change over time. The equipment tested is generally selected by the equipment supplier and has been set up by them. It should be noted that individual centres may be set up differently for example to meet the requirements of the screening service.

The technical image quality as measured on this system must be acceptable. The image quality of the final displayed image will be affected by the image processing and display and this is separately evaluated qualitatively in the Practical Evaluation.

This evaluation report does not absolve the provider of their responsibility during the procurement process to ensure the equipment is suitable for the usage intended by the provider.

# 1. Introduction

## 1.1 Testing procedures and performance standards for digital mammography

This report is one of a series evaluating commercially available direct digital radiography (DR) systems for mammography on behalf of the NHS Breast Screening Programme (NHSBSP) [1] [2] [3] [4] [5]. The testing methods and standards applied are mainly derived from NHSBSP Equipment Report 0604 [6] which is referred to in this document as 'the NHSBSP protocol'. The standards for image quality and dose are the same as those provided in the European protocol, [7] [8] but the latter has been followed where it provides a more detailed standard, for example, for the automatic exposure control (AEC) system.

Some additional tests were carried out according to the UK recommendations for testing mammography X-ray equipment as described in IPEM Report 89 [9].

## 1.2 Objectives

The aims of the evaluation were:

- to determine whether the Hologic Envision digital mammography system, operating in 2D mode, meets the main standards in the NHSBSP and European protocols
- to provide performance data for comparison against other systems.

# 2. Methods

## 2.1 System tested

The tests were conducted at the Hologic factory in Newark, Delaware, United States of America on a Hologic Envision system as described in Table 1. The Envision is shown in Figure 1.

**Table 1. System description**

| | |
|---|---|
| Manufacturer | Hologic |
| Model | Envision |
| System serial number | GAN300000105 |
| Target material | Tungsten (W) |
| Added filtration | 50µm Rhodium (Rh), 50µm Silver (Ag), [700µm Aluminium (Al) and 300µm Copper (Cu) used for tomosynthesis and contrast enhanced mammography respectively] |
| Detector type | Amorphous selenium |
| Detector serial number | PRPV012 |
| Pixel pitch | 70µm |
| Detector size | 232.96 mm x 286.72 mm |
| Pixel array | 3328 x 4096 |
| Typical image sizes | 16.2 MB (179.20 mm x 232.96 mm field size)<br>26.0 MB (232.96 mm x 286.72 mm field size) |
| Source to detector distance | 700mm |
| Source to table distance | 675mm |
| Preliminary exposure mAs | ≤ 5mAs for CBT < 45mm otherwise ≤ 10mAs<br><br>Between 3 and 10mAs up to 65mm, and 10mAs thereafter |
| Automatic exposure control (AEC) modes | Auto filter, Auto time |
| Sensor selection options | Auto (auto-sensor or auto-mean), manual |
| Software version | AWS:1.1.0.698 |

The AEC system splits the image acquired during the preliminary exposure into a matrix of 128 pixel by 128 pixel regions. The AEC system will select two of these regions based on the mode selected:

- In auto-sensor mode the two most attenuated regions in the breast are used.

- In auto-mean mode one region is chosen over the most attenuated region in the breast whilst the other is positioned at the point most representative of the average breast attenuation.

In both modes the final exposure settings are based on the average pixel values within the two automatically selected regions. The default setting is auto-sensor (and used in this report unless otherwise stated). Selection of auto-mean can be set by the Hologic field service engineer upon request.

The detector of the Envision uses the same technology as the 3Dimensions with the same pixel spacing. The read out electronics have been improved to allow faster readout times but Hologic state that technical quality metrics of the detector like, MTF and DQE, should remain similar.

**Figure 1. The Hologic Envision system**

## 2.2 Image processing

The Envision has several options for the image processing. The settings include for example changes of image sharpness and image contrast. These are set by the service engineer, these are not tested in this report.

## 2.3 Output and HVL

The output and half-value-layer (HVL) were measured as described in the NHSBSP protocol [9], at intervals of 3kV.

## 2.4 Detector response

The detector response was measured with a 2 mm thick aluminium sheet at the tube head. The grid and paddle were removed and a dosimeter was positioned above the breast support, 50mm from the chest wall edge (CWE). The incident air kerma was measured for a range of manually set mAs values at 29kVp W/Rh anode/filter combination. The readings were corrected to the surface of the detector using the inverse square law. No correction was made for attenuation by the detector housing. A 10mm x 10mm region of interest (ROI) was positioned on the midline, 50mm from the CWE of each image. The average pixel value and the standard deviation of pixel values within the ROI were measured. The relationship between average pixel values and the incident air kerma to the detector was determined.

## 2.5 Dose estimation

Doses were measured by exposing different thicknesses of PMMA under AEC. Each PMMA block had an area of 180mm x 240mm. No compression was required for imaging and so the paddle height was adjusted to be equal to the equivalent breast thickness, as shown in Table 3. The exposure factors were noted and mean glandular doses (MGDs) were calculated for breasts of equivalent thicknesses using the Dance dosimetry model [10] [11] [12].

Although not yet adopted in UK breast screening programmes, a joint AAPM TG282 and EFOMP report on breast dosimetry was published recently [13]. The model proposed in this collaboration is intended by the authors as a future international standard. Mean glandular doses were therefore also estimated and tabulated using the TG282 model for cranio-caudal (CC) views applying TG282 median percentile glandularities.

An aluminium square, 10mm x 10mm and 0.2mm thick, was used with the PMMA during these exposures, so that the images produced could be used for the calculation of the signal difference to noise ratio (SDNR), described in Section 2.6. The aluminium square was placed between two 10mm thick slabs of 180mm x 240mm PMMA, on the midline, with its centre 50mm from the CWE. Additional layers of PMMA were placed on top to vary the total thickness.

## 2.6 Signal difference to noise ratio

Unprocessed images acquired during the dose measurement were analysed to obtain the SDNRs. Thirty-six small square ROIs (approximately 2.5mm x 2.5mm) were used to determine the average signal and the standard deviation in the signal within the image of the aluminium square (4 ROIs) and the surrounding background (32 ROIs), as shown in Figure 2. Small ROIs are used to minimise distortions due to the heel effect and other causes of non-uniformity [14]. The SDNR was calculated for each image, as defined in the NHSBSP and European Protocols.

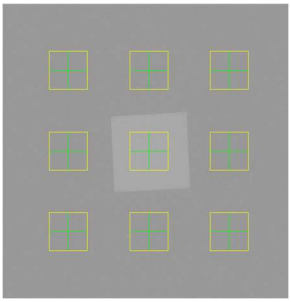

**Figure 2. Location and size of ROIs used to determine the SDNR**

To apply the standards in the European protocol, it is necessary to relate the image quality measured using the CDMAM (Section 2.9) for an equivalent breast thickness of 60mm, to that for other breast thicknesses. The European protocol [8] gives the relationship between threshold contrast and SDNR measurements, enabling the calculation of a target SDNR value for a particular level of image quality. This can be compared to SDNR measurements made at other breast thicknesses. Contrast for a particular gold thickness is calculated using Equation 1, and target SDNR is calculated using Equation 2.

$$\text{Contrast} = 1 - e^{-\mu t} \quad (1)$$

where μ is the effective attenuation coefficient for gold, and t is the gold thickness.

$$SDNR_{target} = \frac{SDNR_{measured} \times TC_{measured}}{TC_{target}} \quad (2)$$

where $SDNR_{measured}$ is the SDNR for a 60mm equivalent breast, $TC_{measured}$ is the threshold contrast calculated using the threshold gold thickness for a 0.1mm diameter detail, (measured using the CDMAM at the same dose as used for $SDNR_{measured}$), and $TC_{target}$ is the calculated threshold contrast corresponding to the threshold gold thickness required to

meet either the minimum acceptable or achievable level of image quality as defined in the NHSBSP protocol.

The threshold gold thickness for the 0.1mm diameter detail is used here because it is generally regarded as the most critical of the detail diameters for which performance standards are set.

The effective attenuation coefficient for gold used in Equation 1 depends on the beam quality used for the exposure, and the value used is in Table 2. This value was calculated with 3mm PMMA representing the compression paddle, using spectra from Hernandez et al [15] and attenuation coefficients for materials in the test objects (aluminium, gold, PMMA) from Berger et al [16].

The European protocol also defines a limiting value for SDNR, which is calculated as a percentage of the threshold contrast for minimum acceptable image quality for each thickness. This limiting value varies with thickness, as shown in Table 3.

**Table 2. Effective attenuation coefficient for gold contrast details in the CDMAM**

| kVp | Target/filter | Effective attenuation coefficient ($\mu m^{-1}$) |
|---|---|---|
| 31 | W/Rh | 0.1252 |

**Table 3. Limiting values for relative SDNR**

| Thickness of PMMA (mm) | Equivalent breast thickness (mm) | Limiting values for relative SDNR (%) in European protocol |
|---|---|---|
| 20 | 21 | > 115 |
| 30 | 32 | > 110 |
| 40 | 45 | > 105 |
| 45 | 53 | > 103 |
| 50 | 60 | > 100 |
| 60 | 75 | > 95 |
| 70 | 90 | > 90 |

The target SDNR values for minimum acceptable and achievable levels of image quality and European limiting values for SDNR were calculated. These were compared with the measured SDNR results for all breast thicknesses.

## 2.7 AEC performance for local dense areas

Instead of the EUREF protocol version of this test performed in past technical evaluations, the European Federation of Organisations for Medical Physics (EFOMP) Digital Breast Tomosynthesis (DBT) protocol [17] was adopted here. This has a number of advantages including simulating a more representative breast thickness and density, quicker testing, and harmonisation of the 2D and DBT setup.

Images of a 40mm thick block of PMMA of size 180mm x 240mm, were acquired under AEC. To simulate local dense regions, extra pieces of PMMA between 4 and 12mm thick and of size 20mm x 40mm were added. The aluminium used in the signal difference to noise ratio (SDNR) test was positioned as shown in Figure 3. The compression plate remained in position at a height of 50mm. The simulated dense area was positioned 50mm from the CWE of the breast support table.

The SDNR, was calculated for each image ensuring the background ROIs were all within the PMMA representing the local dense region.

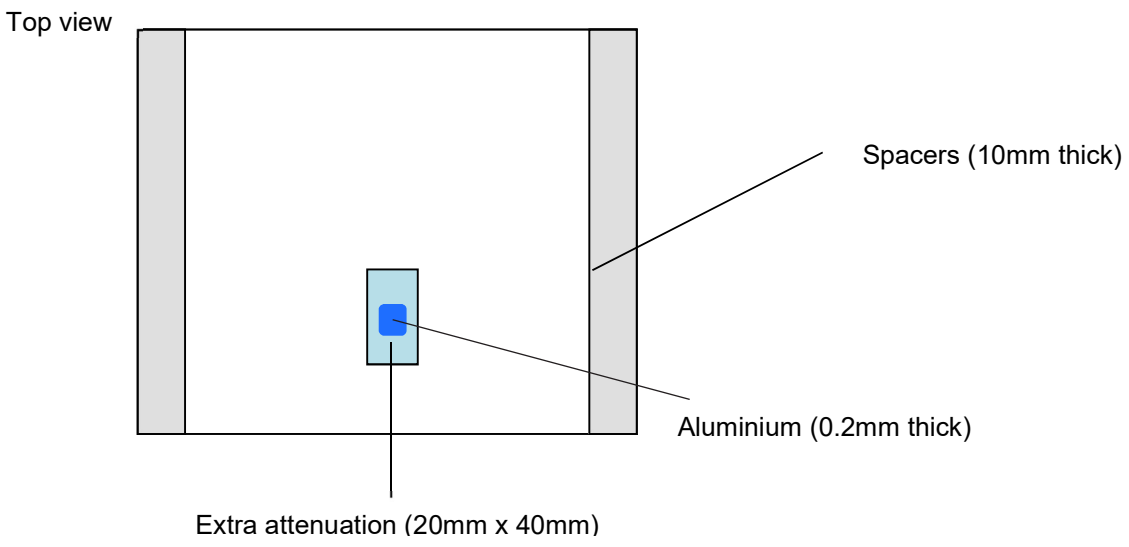

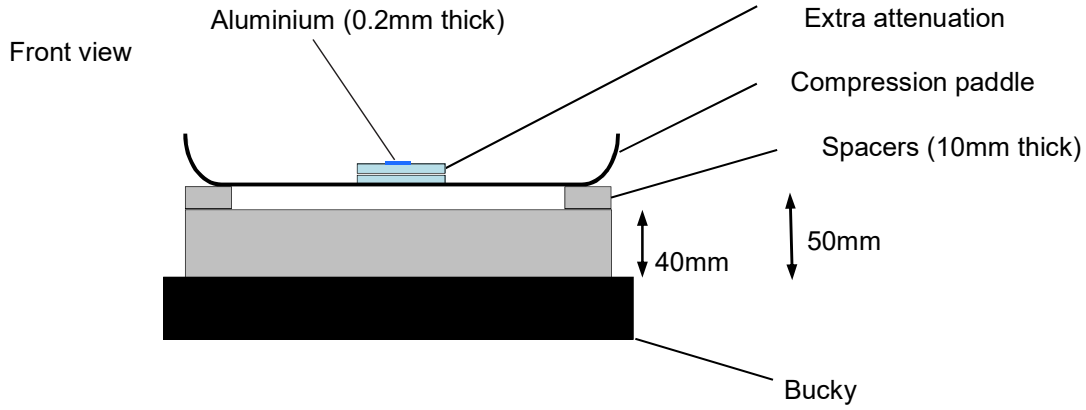


**Figure 3. Setup to measure AEC performance for local dense areas**

## 2.8 Noise analysis

The images acquired in the measurements of detector response, using 29kVp W/Rh, were used to analyse the image noise. Small ROIs with an area of approximately 2.5mm x 2.5mm were placed on the midline, 50mm from the CWE. The average of the standard deviations of the pixel values in each of the ROIs for each image were used to investigate the relationship between the air kerma incident to the detector and the image noise. A power fit of standard deviation against incident air kerma was made. If electronic and structure noise are small, then a square root relationship is expected. It was assumed that the noise in the image comprises three components: electronic noise, structural noise, and quantum noise. The relationship between them is shown in Equation 3:

$$\sigma_p = \sqrt{k_e^2 + k_q^2 p + k_s^2 \mathrm{p}^2} \qquad (3)$$

where $\sigma_p$ is the standard deviation in pixel values within an ROI with a uniform exposure and a mean pixel value $p$, and $k_e$, $k_q$, and $k_s$ are the coefficients determining the amount of electronic, quantum, and structural noise in a pixel with a value $p$. This method of analysis has been described previously [18]. For simplicity, the noise is generally presented here as relative noise defined as in Equation 4.

$$\text{Relative noise} = {}^{\sigma_p}/_{p} \qquad (4)$$

The variation in relative noise with mean pixel value was evaluated and fitted using Equation 3, and non-linear regression used to determine the best fit for the constants and their asymptotic confidence limits (using Graphpad Prism version 7.00 for Windows, Graphpad software, San Diego, California, USA, www.graphpad.com). This established whether the

experimental measurements of the noise fitted this equation, and the relative proportions of the different noise components. The relationship between noise and pixel values has been found empirically to be approximated by a simple power relationship as shown in Equation 5.

$$\sigma_p/_p = k_t p^{-n} \quad (5)$$

where $k_t$ is a constant. If the noise were purely quantum noise the value of n would be 0.5. However, the presence of electronic and structural noise means that *n* can be slightly higher or lower than 0.5. For graphical presentation in this report, pixel values were converted to incident air kerma at the detector using the detector response data described in section 2.3.

The variance in pixel values within a ROI is defined as the standard deviation squared. The total variance against incident air kerma at the detector was fitted using Equation 3. Non-linear regression was used to determine the best fit for the constants and their asymptotic confidence limits, using the Graphpad Prism software.

Using the calculated constants, the structural, electronic, and quantum components of the variance were estimated, assuming that each component was independently related to incident air kerma. The percentage of the total variance represented by each component was then calculated and plotted against incident air kerma at the detector.

## 2.9 Image quality measurements

Contrast detail measurements were made using a CDMAM phantom (serial number 1022, version 3.4, UMC St. Radboud, Nijmegen University, Netherlands). The phantom was positioned with a 20mm thickness of PMMA above and below, to give a total attenuation approximately equivalent to 50mm of PMMA or 60mm thickness of typical breast tissue. The exposure factors were chosen to match as closely as possible those selected by the AEC, at the standard dose setting, when imaging a 50mm thickness of PMMA. This procedure was repeated to obtain a representative sample of 16 images at this dose level. Further sets of 16 images of the test phantom were then obtained at other dose levels by manually selecting higher and lower mAs values with the same beam quality.

The CDMAM images were read and analysed automatically using Version 1.6 of CDCOM [19] [20]. and Version 2.1.0 of CDMAM Analysis (https://medphys.royalsurrey.nhs.uk/nccpm/). The threshold gold thickness for a typical human observer was predicted using Equation 6.

$$TC_{predicted} = rTC_{auto} \quad (6)$$

where $TC_{predicted}$ is the predicted threshold contrast for a typical observer, $TC_{auto}$ is the threshold contrast measured using an automated procedure with CDMAM images. r is the average ratio between human and automatic threshold contrast determined experimentally with the values shown in Table 4.

**Table 4. Values of r used to predict threshold contrast**

| Diameter of gold disc (mm) | Average ratio of human to automatically measured threshold contrast (r) |
|---|---|
| 0.08 | 1.40 |
| 0.10 | 1.50 |
| 0.13 | 1.60 |
| 0.16 | 1.68 |
| 0.20 | 1.75 |
| 0.25 | 1.82 |
| 0.31 | 1.88 |
| 0.40 | 1.94 |
| 0.50 | 1.98 |
| 0.63 | 2.01 |
| 0.80 | 2.06 |
| 1.00 | 2.11 |

The predicted threshold gold thickness for each detail diameter in the range 0.1mm to 1.0mm was fitted with a curve for each dose level, using the relationship shown in Equation 7.

$$\text{Threshold gold thickness} = a + bx^{-1} + cx^{-2} + dx^{-3} \quad (7)$$

where x is the detail diameter, and *a*, *b*, *c* and *d* are coefficients adjusted to obtain a least squares fit.

The confidence limits for the predicted threshold gold thicknesses have been previously determined by a sampling method using a large set of images. The threshold contrasts quoted in the tables of results are derived from the fitted curves.

The expected relationship between threshold contrast and MGD is shown in Equation 8.

$$\text{Threshold contrast} = \lambda D^{-n} \quad (8)$$

where *D* is the MGD for a 60mm thick standard breast (equivalent to the test phantom configuration used for the image quality measurement), and λ is a constant to be fitted.

It is assumed that a similar equation applies when using threshold gold thickness instead of contrast. This equation was plotted with the experimental data for detail diameters of 0.1 and

0.25mm. The value of *n* resulting in the best fit to the experimental data was determined, and the doses required for target SDNR values were calculated for data relating to these detail diameters.

The MGDs to reach the minimum and achievable image quality standards in the NHSBSP protocol were then estimated. The error in estimating these doses depends on the accuracy of the curve fitting procedure, and pooled data for several systems has been used to estimate 95% confidence limits of about 20%.

## 2.10 Quantitative measurements

The modulation transfer function (MTF), normalised noise power spectrum (NNPS) and the detective quantum efficiency (DQE) of the system were measured. The methods used were as close as possible to those described by the International Electrotechnical Commission (IEC) [21], but as the measurements are undertaken using a mammographic unit, there are some compromises and the results are affected by the system. The radiation quality used for the measurements was adjusted by placing a uniform 2mm thick aluminium filter at the tube housing. The beam quality used was 29kVp W/Rh anode/filter combination. The test device to measure the MTF comprised a 120mm x 60mm rectangle of stainless steel with a polished straight edge, of thickness 2mm. This test device was placed directly on the breast support table, and the grid was removed. The test device was positioned to measure the MTF in two directions, first almost perpendicular to the CWE and then almost parallel to it.

To measure the noise power spectrum the test device was removed and exposures made for a range of incident air kerma at the surface of the table. The DQE is presented as the average of measurements in the directions perpendicular and parallel to the CWE.

## 2.11 Other tests

Other tests carried out included tests prescribed in IPEM Report 89 [9] for mammographic X-ray sets, as well as those in the NHSBSP protocol for digital mammographic systems. In addition to the five ROI method for uniformity described in these documents, uniformity was also assessed using a sliding ROI of size 2mm by 2mm.

# 3. Results

## 3.1 Output and HVL

The output and HVL measurements are shown in Table 5.

**Table 5. Output and HVL**

| kVp | Target/filter | Output (μGy/mAs at 1m) | HVL (mm Al) |
|---|---|---|---|
| 23 | W/Rh | 7.0 | 0.44 |
| 26 | W/Rh | 10.9 | 0.49 |
| 29 | W/Rh | 14.8 | 0.53 |
| 32 | W/Rh | 18.8 | 0.56 |
| 35 | W/Rh | 22.8 | 0.59 |
| 38 | W/Rh | 26.9 | 0.60 |
| 23 | W/Ag | 8.2 | 0.43 |
| 26 | W/Ag | 13.6 | 0.49 |
| 29 | W/Ag | 18.9 | 0.55 |
| 32 | W/Ag | 24.3 | 0.60 |
| 35 | W/Ag | 29.6 | 0.65 |
| 38 | W/Ag | 35.0 | 0.70 |

## 3.2 Detector response

The detector response is shown in Figure 4.

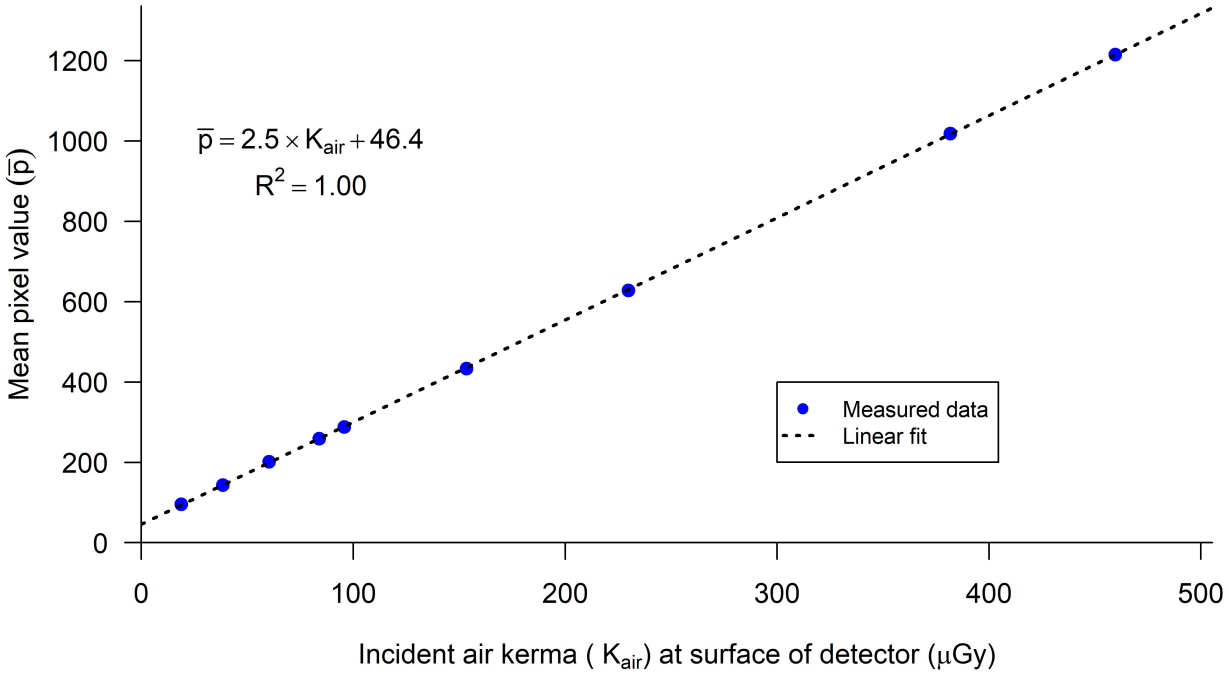


**Figure 4. Detector response acquired at 29kVp W/Rh anode/filter combination with 2mm Al at the tube port**

## 3.3 AEC performance

### 3.3.1 Dose

The MGDs for breasts simulated with PMMA exposed under AEC are shown in Table 6 for exposures made in grid mode with AutoFilter and AEC sensor position 2 (the aluminium was outside of this region). The mAs values in Table 6 include the preliminary exposure, the values of the preliminary exposure can be found in Table 7. The preliminary exposures are not in the DICOM header but were calculated from other values in the header. The MGDs were calculated from the total mAs, including the preliminary exposure. The results presented in Table 6, are also presented graphically in Figure 5.

**Table 6. MGD for simulated breasts (grid in, AutoFilter, 24x29 paddle)**

| PMMA thick-ness (mm) | Equiv-alent breast thickness (mm) | kVp | Target/ filter | mAs | Dance MGD (mGy) | Remedial dose level (mGy) | Displ-ayed dose (mGy) | TG282 MGD (mGy) |
|---|---|---|---|---|---|---|---|---|

| | | | | | | | | |
|---|---|---|---|---|---|---|---|---|
| 20 | 21 | 25 | W/Rh | 52.3 | 0.56 | 1.0 | 0.59 | 0.57 |
| 30 | 32 | 26 | W/Rh | 79.7 | 0.79 | 1.5 | 0.77 | 0.80 |
| 40 | 45 | 28 | W/Rh | 101.1 | 1.08 | 2.0 | 1.01 | 1.03 |
| 45 | 53 | 29 | W/Rh | 123.9 | 1.36 | 2.5 | 1.32 | 1.22 |
| 50 | 60 | 31 | W/Rh | 147.1 | 1.85 | 3.0 | 1.78 | 1.56 |
| 60 | 75 | 31 | W/Ag | 164.4 | 2.51 | 4.5 | 2.51 | 1.93 |
| 70 | 90 | 34 | W/Ag | 157.3 | 2.83 | 6.5 | 2.93 | 1.97 |
| 80 | 103 | 36 | W/Ag | 163.9 | 3.16 | - | 3.30 | 1.99 |

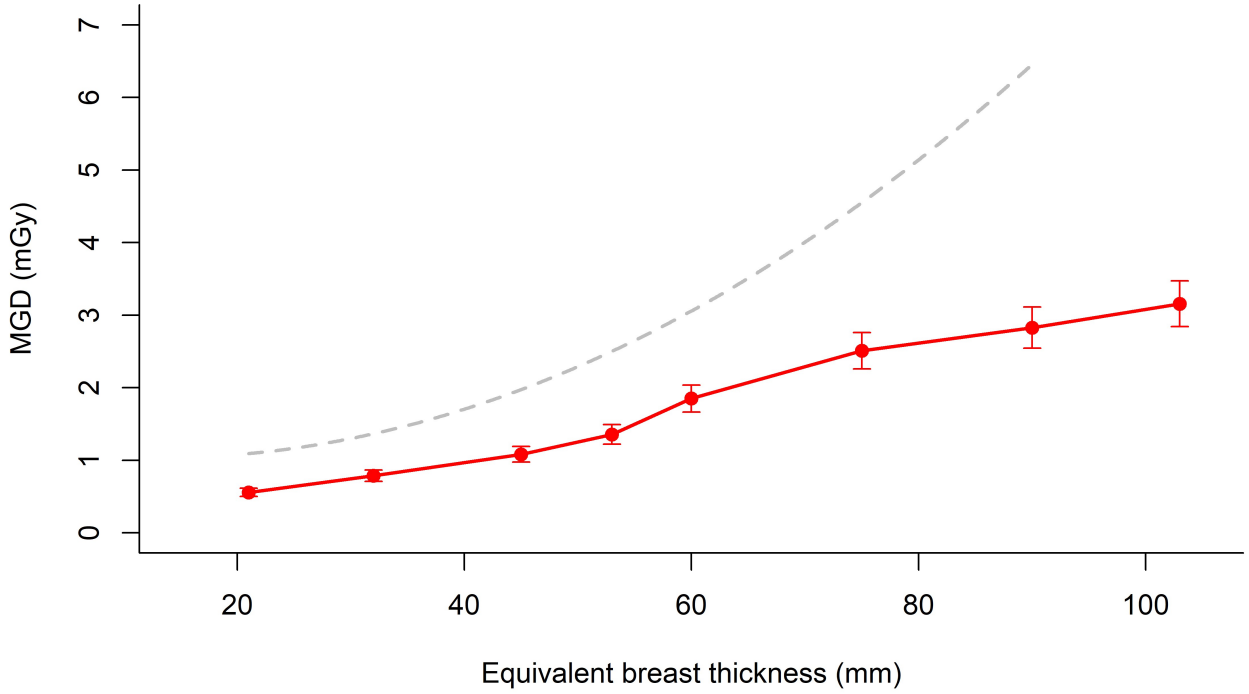

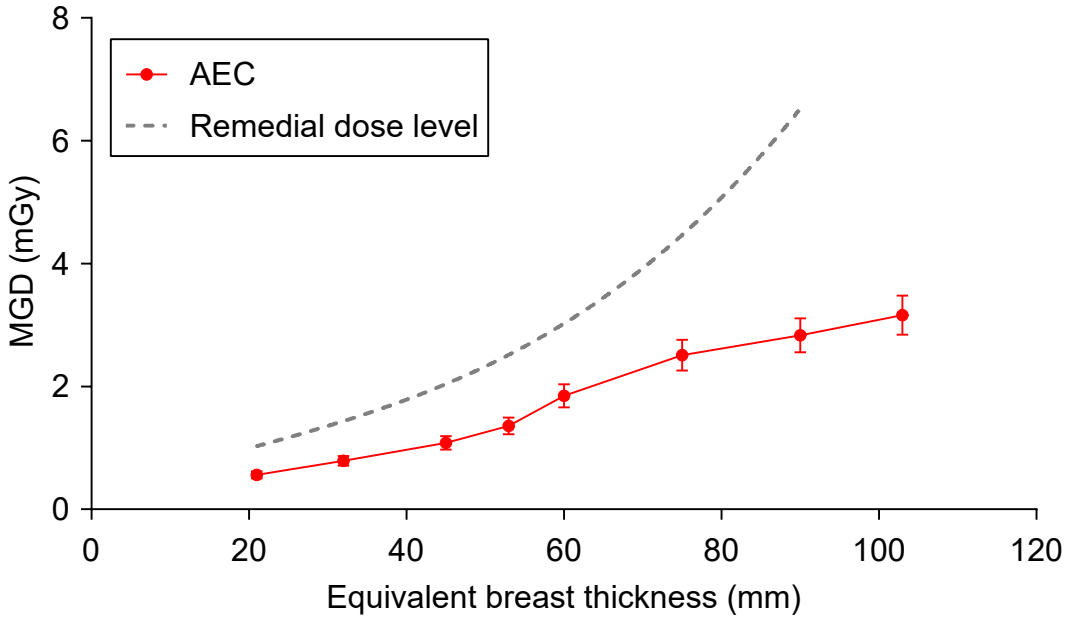


**Figure 5. Dance MGD for different thicknesses of simulated breasts using AEC normal dose mode. (Error bars indicate 95% confidence limits)**

**Table 7. Preliminary exposure mAs under AEC**

| PMMA thickness (mm) | Equivalent breast thickness (mm) | kVp | Target/ filter | Total mAs | Preliminary exposure mAs | mAs of image |
|---|---|---|---|---|---|---|
| 20 | 21 | 25 | W/Rh | 52.3 | 3.0 | 49.3 |
| 30 | 32 | 26 | W/Rh | 79.7 | 4.0 | 75.7 |
| 40 | 45 | 28 | W/Rh | 101.1 | 6.0 | 95.1 |
| 45 | 53 | 29 | W/Rh | 123.9 | 7.0 | 116.9 |
| 50 | 60 | 31 | W/Rh | 147.1 | 8.9 | 138.2 |
| 60 | 75 | 31 | W/Ag | 164.4 | 9.9 | 154.5 |
| 70 | 90 | 34 | W/Ag | 157.3 | 10.0 | 147.3 |
| 80 | 103 | 36 | W/Ag | 163.9 | 9.9 | 154.0 |

### 3.3.2 Signal difference to noise ratio

The results of the SDNR measurements for exposures made in grid mode with AutoFilter on in 2D are in Table 8 and in Figure 6. The following calculated values are also shown:

- SDNR to meet the minimum acceptable image quality standard
- SDNR to meet the achievable image quality standard

- SDNRs at each thickness to meet the limiting value in the European protocol

**Table 8. SDNR measurements (grid in, AutoFilter, 24x29 paddle)**

| PMMA (mm) | Equivalent breast thickness (mm) | Measured SDNR | SDNR for minimum acceptable IQ | SDNR for achievable IQ | European limiting SDNR value |
|---|---|---|---|---|---|
| 20 | 21 | 9.2 | 3.2 | 4.8 | 3.7 |
| 30 | 32 | 8.3 | 3.2 | 4.8 | 3.6 |
| 40 | 45 | 7.5 | 3.2 | 4.8 | 3.4 |
| 45 | 53 | 7.3 | 3.2 | 4.8 | 3.3 |
| 50 | 60 | 7.0 | 3.2 | 4.8 | 3.2 |
| 60 | 75 | 6.7 | 3.2 | 4.8 | 3.1 |
| 70 | 90 | 5.4 | 3.2 | 4.8 | 2.9 |
| 80 | 103 | 4.2 | 3.2 | 4.8 | 2.9 |

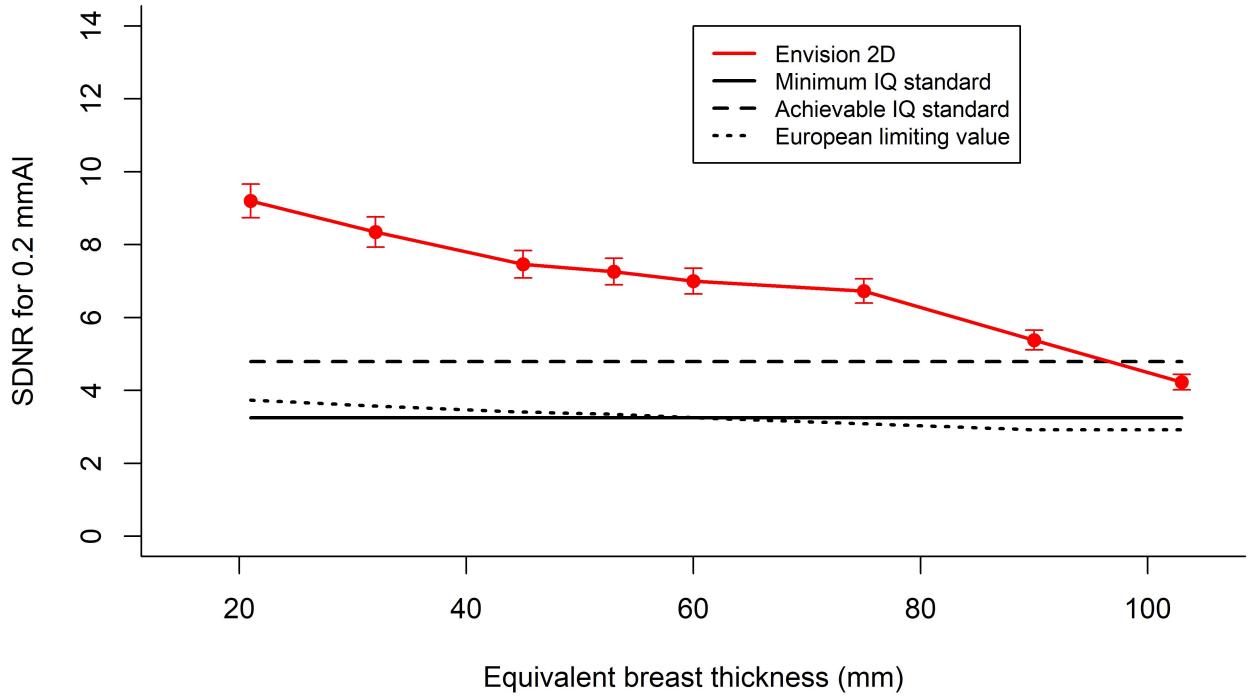


**Figure 6. Measured SDNR compared with the limiting values in the European protocol. (Error bars indicate 95% confidence limits.)**

### 3.3.3 AEC performance for local dense areas

It is expected that when the AEC adjusts for local dense areas, the SDNR remains constant with increasing thickness of extra PMMA. The results presented in Table 9 and Figure 7

show that the SDNR does remain constant as thickness increases up to a total attenuation of 52mm PMMA. It should be noted that the response of the AEC in this test varies with the position of the aluminium relative to the sampling matrix used by the AEC algorithm. The results given here were obtained after aligning the aluminium with the AEC sampling matrix such that there was at least one cell in the matrix completely bounded by the edges of the aluminium square.

**Table 9. AEC performance for local dense areas (Auto Sensor)**

| Total attenuation (mm PMMA) | kVp | Target/ filter | Tube load (mAs) | SDNR | SDNR deviation from 44mm PMMA value (%) |
|---|---|---|---|---|---|
| 40 | 29 | W/Rh | 99.9 | 7.6 | 6.1% |
| 44 | 29 | W/Rh | 126.7 | 7.5 | 0% |
| 48 | 29 | W/Rh | 144.2 | 7 | -9.3% |
| 52 | 29 | W/Rh | 168.9 | 6.6 | -17.8% |

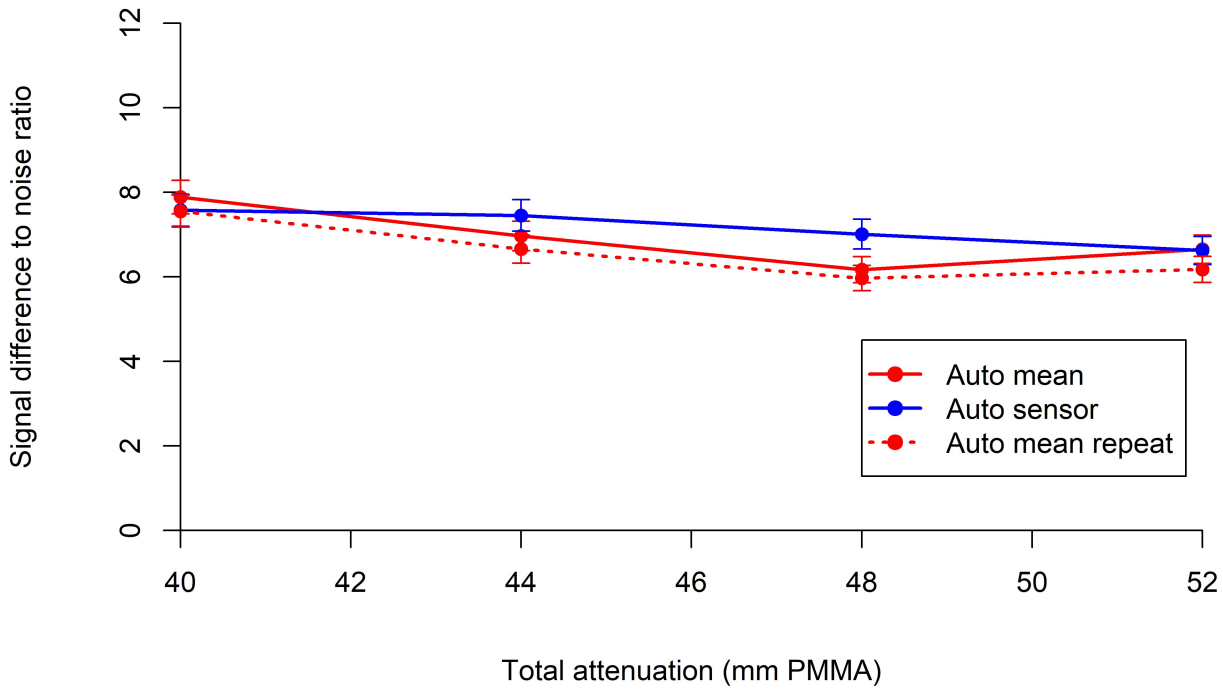


**Figure 7. AEC performance for local dense areas**

## 3.4 Noise measurements

The variation in noise with dose was analysed by plotting the standard deviation in pixel values against the incident air kerma to the detector, as shown in Figure 8. The fitted power

curve has an index of 0.52, which is close to the expected value of 0.5 for quantum noise sources alone.

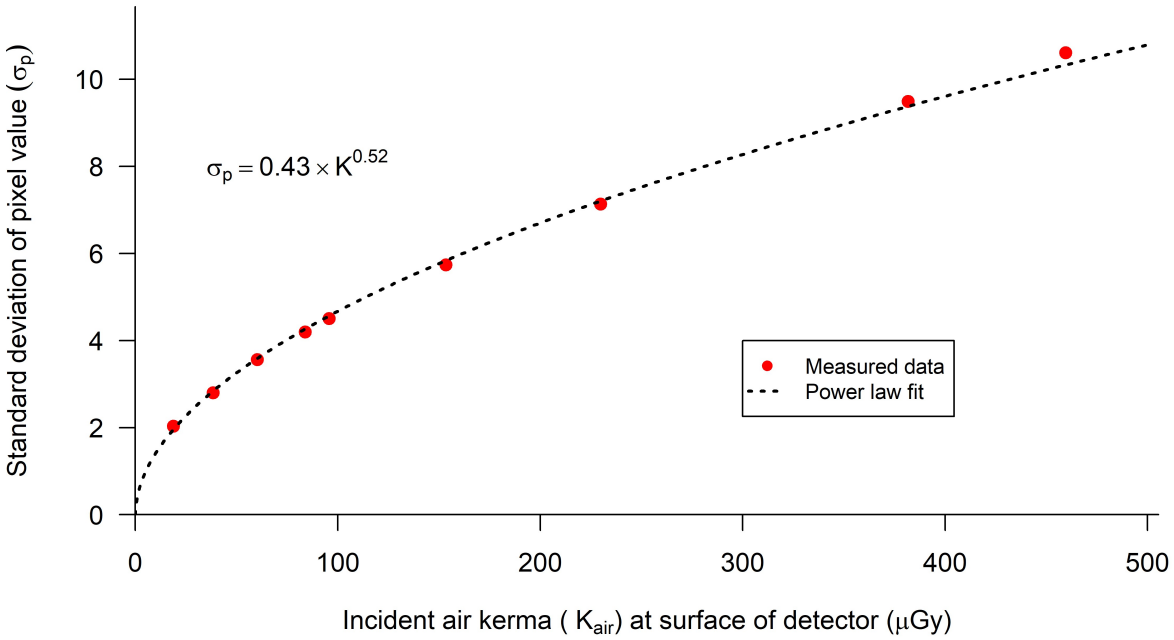


**Figure 8. Standard deviation of linearized pixel values versus incident air kerma at detector**

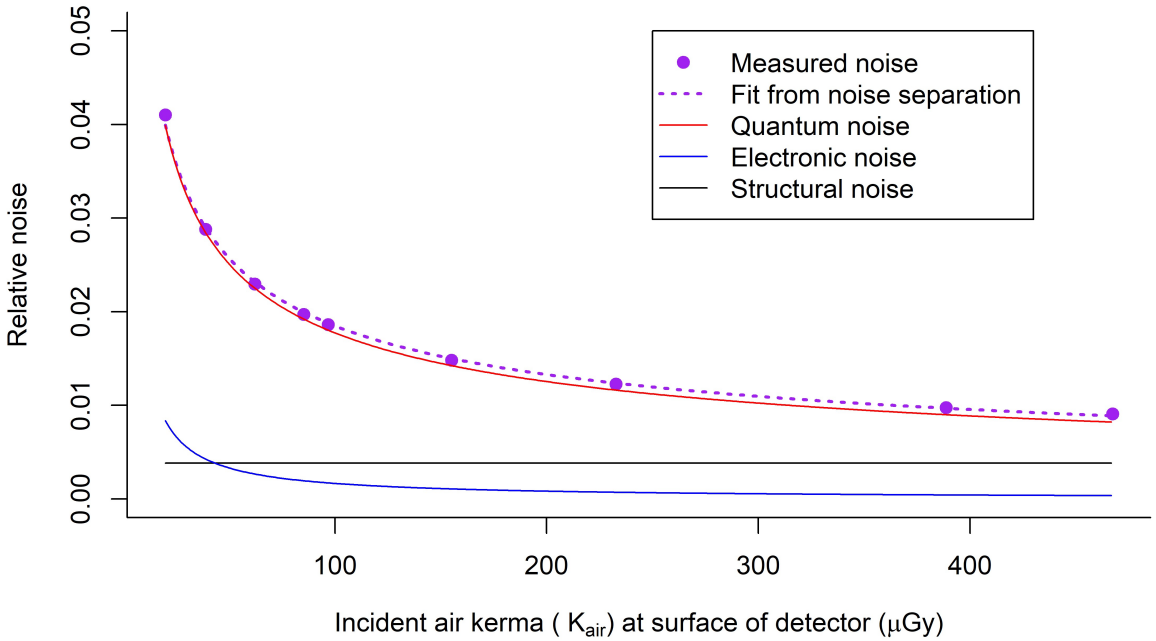


**Figure 9. Relative noise and noise components**

Figure 9 shows the relative noise at different incident air kerma. The estimated relative contributions of electronic, structural, and quantum noise are shown and the quadratic sum of these contributions fitted to the measured noise (using Equation 3).

Figure 10 shows the different amounts of variance due to each component. From this, the dose range over which the quantum component dominates can be seen.

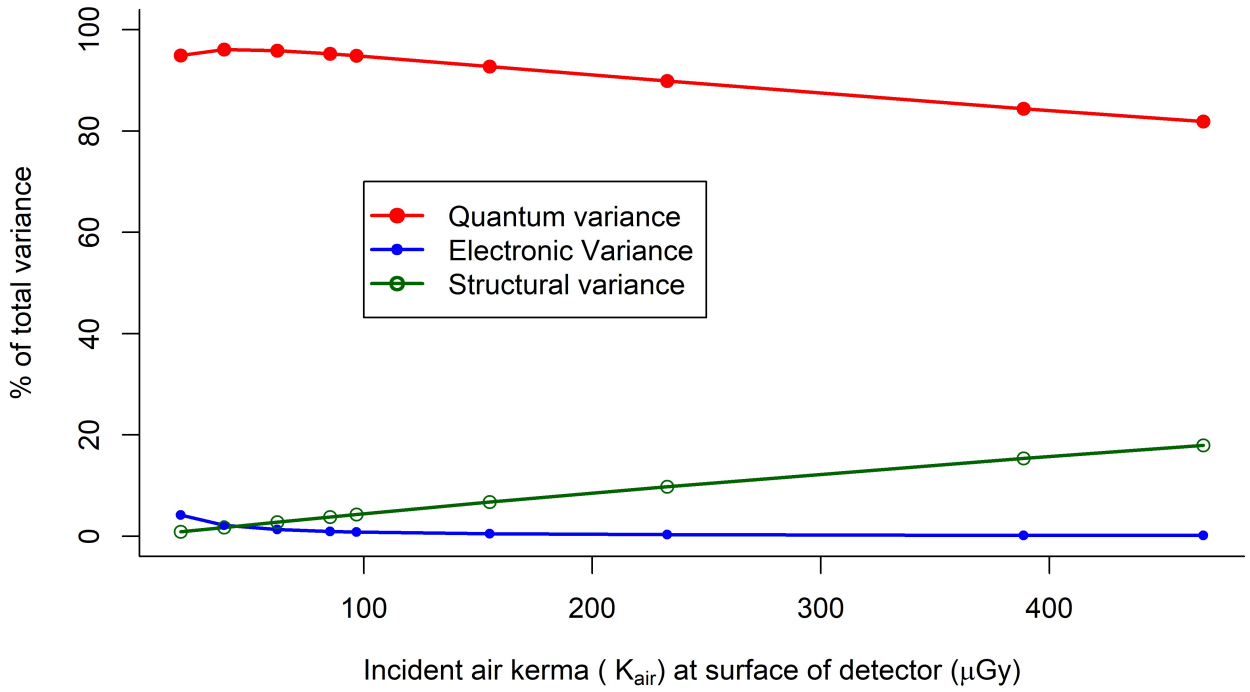


**Figure 10. Noise components as a percentage of the total variance**

## 3.5 Image quality measurements

The exposure factors used for each set of 16 CDMAM images are shown in Table 10. The Dance MGDs were chosen to cover a wide range centred around 1.76 mGy, which was close to that selected for the equivalent breast of 60mm thick in AEC mode.

**Table 10. Images acquired for image quality measurement**

| kVp | Target/filter | Tube loading (mAs) | Mean glandular dose to equivalent breasts 60mm thick (mGy) |
|---|---|---|---|
| 31 | W/Rh | 70.0 (0.5x AEC) | 0.88 |
| 31 | W/Rh | 100.0 (0.7x AEC) | 1.26 |
| 31 | W/Rh | 140.0 (1.0x AEC) | 1.76 |
| 31 | W/Rh | 200.0 (1.4x AEC) | 2.51 |
| 31 | W/Rh | 280.0 (2.0x AEC) | 3.52 |

The contrast detail curves (determined by automatic reading of the images) at the different dose levels are shown in Figure 11. The threshold gold thicknesses measured for different detail diameters at the selected dose levels are shown in Table 11. The NHSBSP minimum acceptable and achievable limits are also shown.

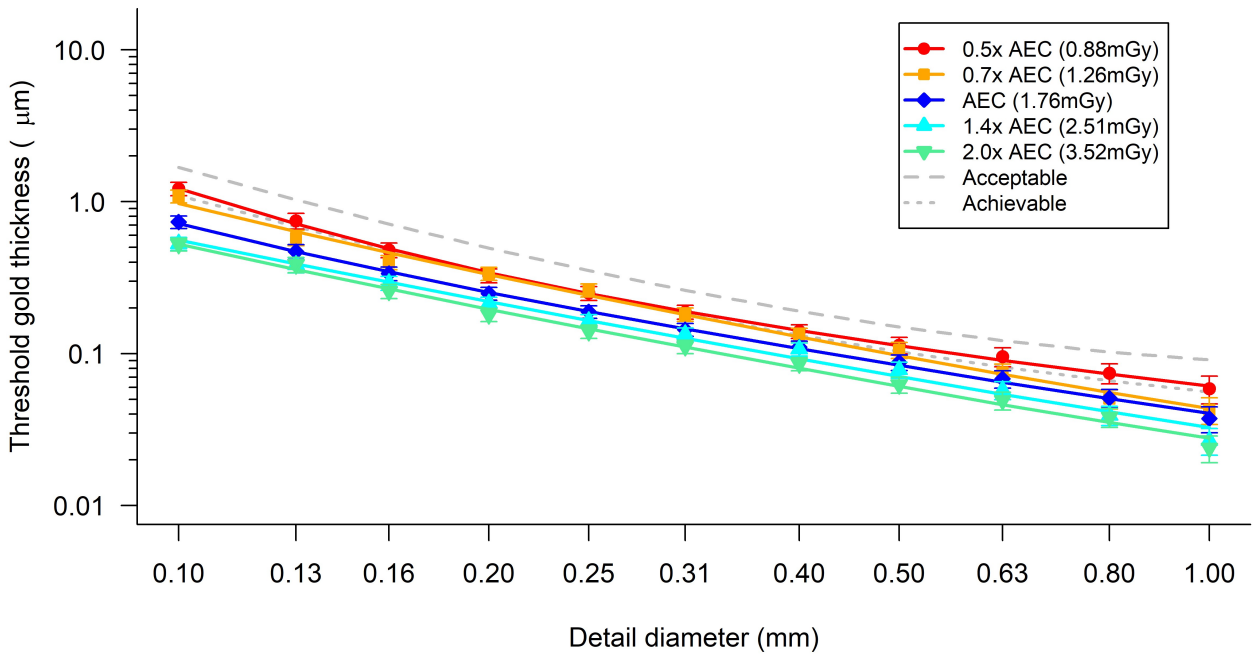


**Figure 11. Threshold gold thickness detection curves for 31kV W/Rh. (Error bars indicate 95% confidence limits.) – CDMAM 3.4**

**Table 11. Average threshold gold thicknesses for different detail diameters 31kVp W/Rh, and automatically predicted data – CDMAM 3.4**

| Diam-eter (mm) | Accept-able value | Achiev-able value | Threshold gold thickness (µm) Mean Glandular Dose to equivalent breast 60mm thick (mGy) 0.88 | 1.26 | 1.76 | 2.51 | 3.52 |
|---|---|---|---|---|---|---|---|
| 0.1 | 1.68 | 1.1 | 1.22 ± 0.12 | 0.97 ± 0.11 | 0.72 ± 0.07 | 0.56 ± 0.05 | 0.53 ± 0.05 |
| 0.25 | 0.352 | 0.244 | 0.25 ± 0.03 | 0.24 ± 0.03 | 0.19 ± 0.02 | 0.17 ± 0.02 | 0.15 ± 0.01 |
| 0.5 | 0.15 | 0.103 | 0.11 ± 0.01 | 0.1 ± 0.01 | 0.08 ± 0.01 | 0.07 ± 0.01 | 0.06 ± 0.01 |
| 1 | 0.091 | 0.056 | 0.06 ± 0.01 | 0.04 ± 0.01 | 0.04 ± 0.01 | 0.03 ± 0.01 | 0.03 ± 0.005 |

The measured threshold gold thicknesses are plotted against the Dance MGD for an equivalent breast for the 0.1mm and 0.25mm detail sizes in Figure 12 from Table 11.

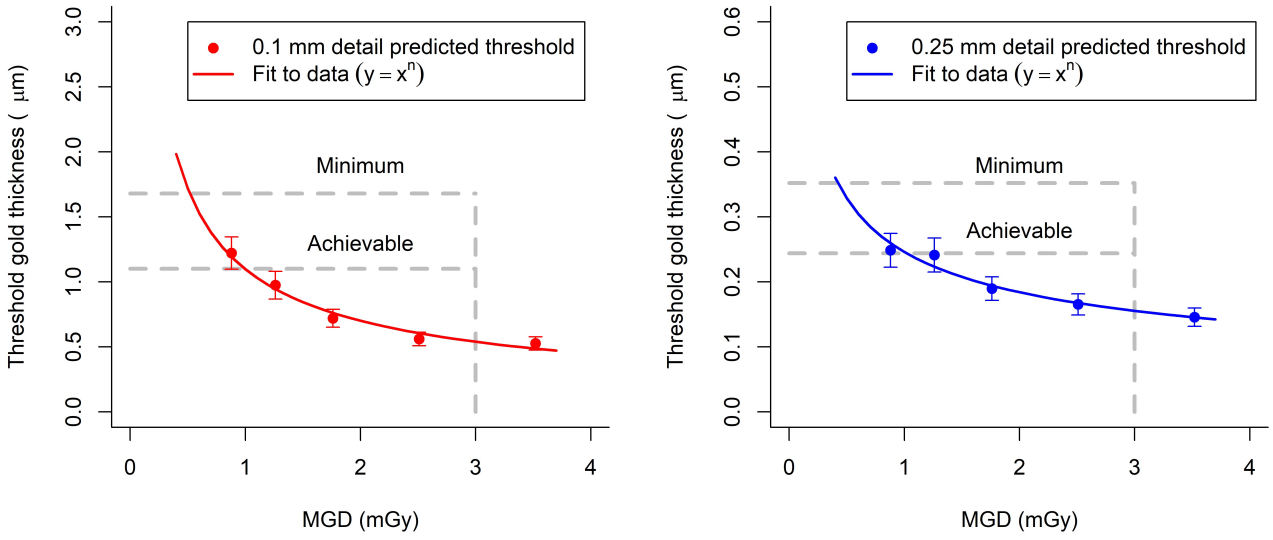


**Figure 12. Threshold gold thickness at different doses. (Error bars indicate 95% confidence limits)**

The Dance MGDs to reach the minimum and achievable image quality standards in the NHSBSP protocol for a 60mm equivalent breast thickness have been estimated from the curves shown in Figure 12. To reach the minimum threshold gold thickness Dance MGDs of 0.54 ± 0.11 mGy and 0.45 ± 0.09 mGy were required for 0.1 mm and 0.25mm details

respectively. To reach the achievable threshold gold thickness Dance MGDs of 1.01 ± 0.20 mGy and 1.04 ± 0.21mGy were required for 0.1mm and 0.25mm details respectively.

## 3.6 Quantitative measurements

The MTF is shown in Figure 13 for the two orthogonal directions. Figure 14 shows the NNPS curves for a range of air kerma incident to the detector. These are measured in the system and so the results will be influenced not only by the detector but the system.

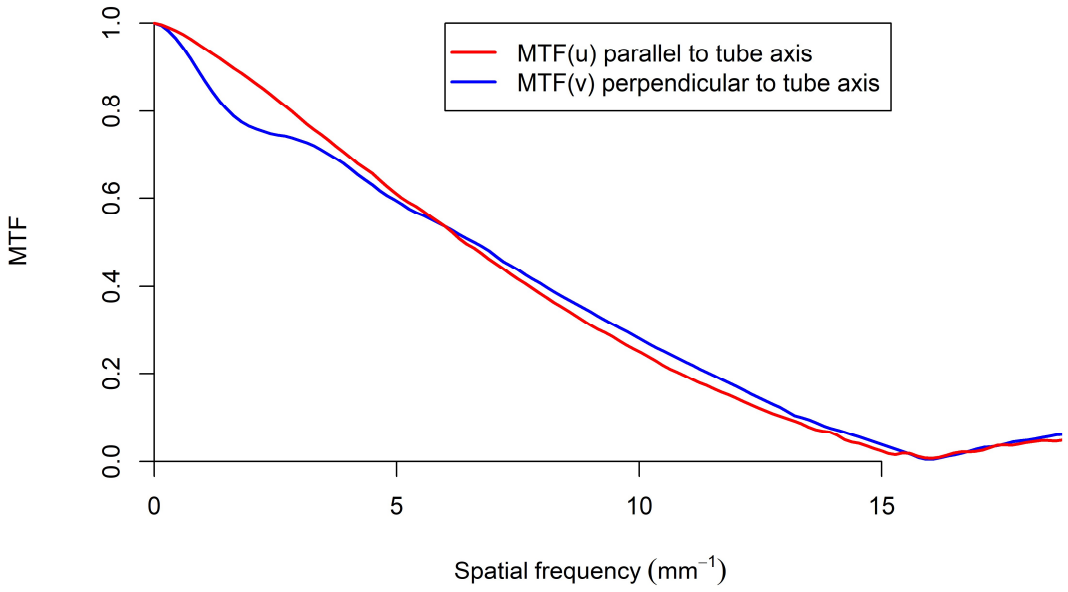


**Figure 13. Pre-sampled MTF**

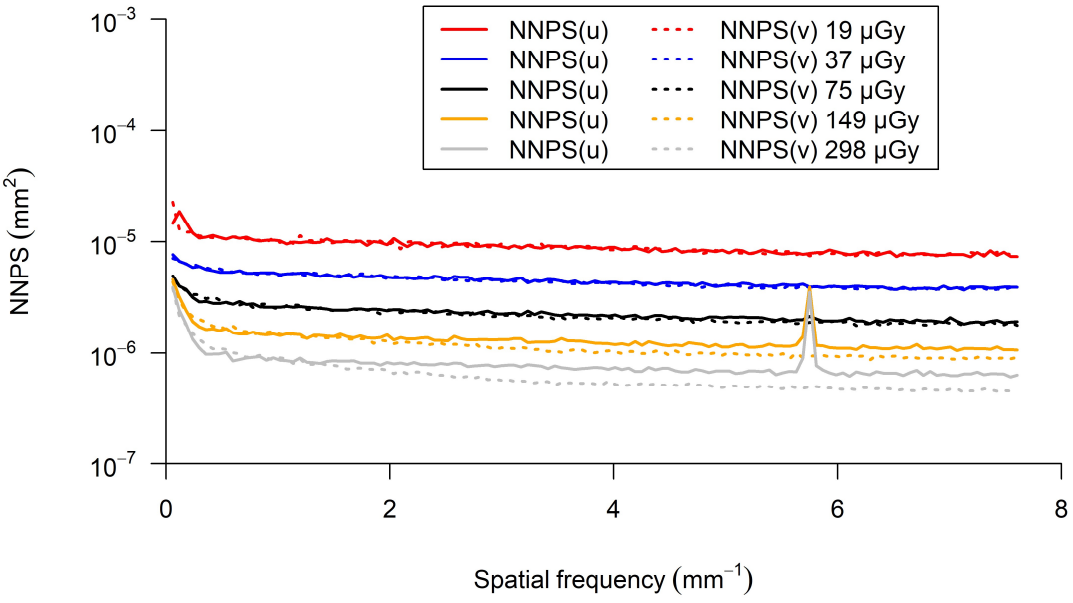

**Figure 14. NNPS curves for a range of air kerma incident to the detector**

Figure 15 shows the DQE averaged in two orthogonal directions for the same beam conditions as used for the NNPS. The spectra of Hernandez et al [15] were attenuated using the Beer-Lambert law with mass attenuation coefficients from Berger et al [16] and the mammographic filter thickness was adjusted iteratively until the calculated HVL matched the results in Table 5. The resulting spectra were used to estimate a *q*-factor of 6100 photons $mm^{-2}$ $\mu Gy^{-1}$. The MTF and DQE measurements were interpolated to show values at standard frequencies in Table 12.

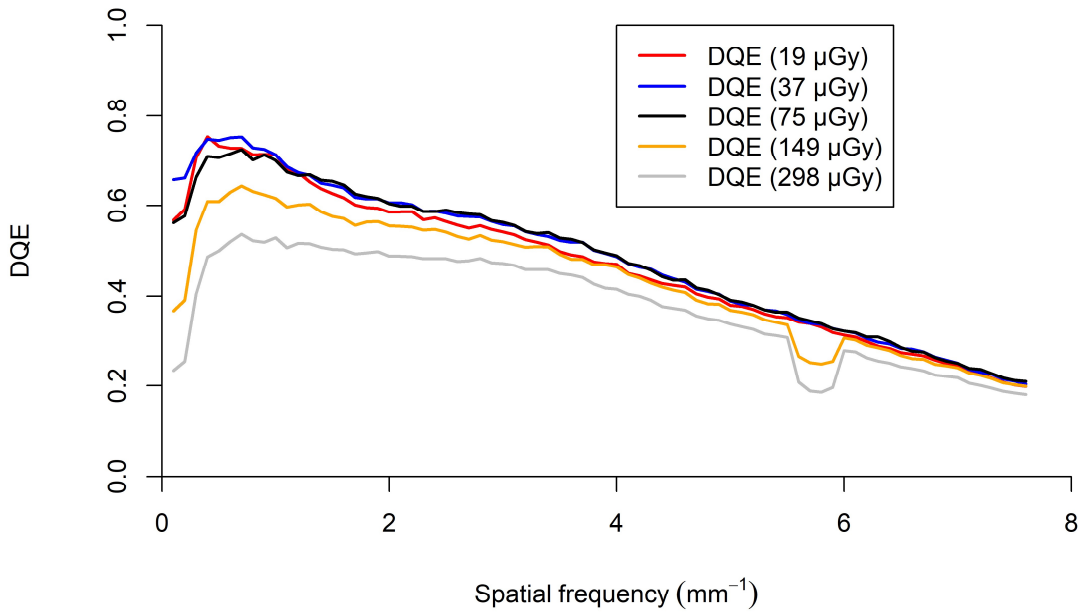


**Figure 15. DQE averaged in both directions for a range of incident air kerma**

**Table 12. MTF and DQE measurements at standard frequencies (DQE at incident air kerma of 75µGy)**

| Frequency ($mm^{-1}$) | MTF (u) | MTF (v) | DQE |
|---|---|---|---|
| 0.0 | 1.00 | 1.00 | - |
| 0.5 | 0.98 | 0.95 | 0.71 |
| 1.0 | 0.95 | 0.88 | 0.70 |
| 1.5 | 0.91 | 0.8 | 0.65 |
| 2.0 | 0.87 | 0.76 | 0.60 |
| 2.5 | 0.83 | 0.75 | 0.59 |
| 3.0 | 0.78 | 0.73 | 0.56 |
| 3.5 | 0.74 | 0.71 | 0.53 |
| 4.0 | 0.7 | 0.67 | 0.49 |
| 4.5 | 0.65 | 0.63 | 0.44 |
| 5.0 | 0.61 | 0.59 | 0.39 |
| 5.5 | 0.58 | 0.56 | 0.36 |
| 6.0 | 0.53 | 0.54 | 0.32 |
| 6.5 | 0.49 | 0.50 | 0.29 |
| 7.0 | 0.46 | 0.47 | 0.25 |
| 7.5 | 0.41 | 0.44 | 0.21 |

## 3.7 Other tests

The results of all the other tests that were carried out were within acceptable limits as prescribed in the NHSBSP protocol [6] and IPEM Report 89 [9].

### 3.7.1 Alignment

Alignment measurements showed that the light field edges were all within 5mm of the edges of the radiation field (IPEM remedial level > 5mm). The radiation field overlapped the edges of the image by up to 4mm (remedial level < 0mm or > 5mm).

### 3.7.2 Image retention

The image retention factor was 0.01, compared to the NHSBSP upper limit of 0.3.

### 3.7.3 AEC repeatability

For a series of 5 repeat images, acquired in quick succession, the maximum deviation of mAs from the mean was 2.9%. The maximum deviation in SNR from the mean was 1.7%. Twenty-three images were acquired at intervals over the five days of testing. Time points were chosen such that some repeats were in the morning before any other exposure whilst

others were immediately after an intensive series of exposures or at the end of the day after a full day of use. The maximum deviation in mAs for these acquisitions was 4.0% - the NHSBSP remedial level is 5%. The maximum deviation in SNR from the mean over the full four days was 2.1%.

### 3.7.4 Uniformity and artefacts

Uniformity images acquired with PMMA on the breast support in the beam showed a variation in pixel values of 0.3% relative to the central area. The NHSBSP remedial level is 10%.

With PMMA the sliding ROI method gave a maximum variation from the mean of 1.0% and a maximum variation from the centre of 1.3%. Figure 16 shows the beam profile as a surface plot for an image of 45mm of PMMA.

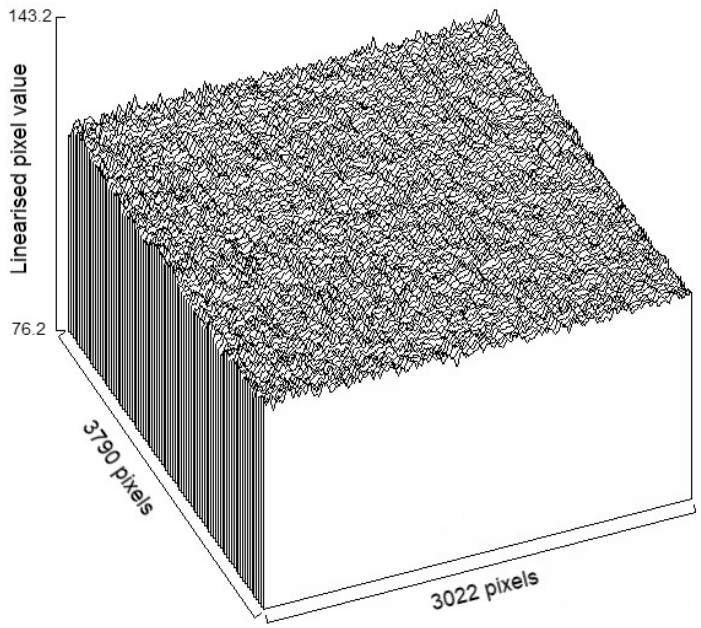


**Figure 16. Beam profile of an image of 45mm PMMA under AEC**

### 3.7.5 Cycle time

For a typical exposure of 45mm PMMA using 29kVp W/Rh and 130mAs, a subsequent exposure could be made 20 seconds after the start of the previous one.

### 3.7.6 Backup timer

When an AEC exposure was attempted with a steel plate blocking the X-ray beam, the exposure terminated after the preliminary exposure. There was no main exposure and no image acquired.

### 3.7.7 Focal spot

The measured dimensions of the broad focal spot were 0.4 mm by 0.5 mm - parallel and perpendicular to the chest wall edge, respectively – compared to a nominal size of 0.3mm. The focal spot dimensions were within the maximum permissible values stated in IEC-60336 [22].

### 3.7.8 Mesh

No discontinuities or blurred regions were seen in the image of the mesh test object.

# 4. Discussion

## 4.1 Dose and signal difference to noise ratio

The detector response was found to be a linear relationship with exposure. This was as expected for Hologic systems.

Dance MGDs measured using PMMA were within the NHSBSP remedial dose levels for all equivalent breast thicknesses. The Dance MGD to the 53mm thick standard breast model was 1.36mGy (Table 6).

The SDNR measurements showed an overall decrease in SDNR with increased thickness of PMMA (Figure 6). Target SDNR values of 3.2 and 4.7, for minimum acceptable and achievable image quality, respectively, were calculated from the SDNR and threshold gold thickness results.

Under AEC, the SDNRs exceeded the target for the achievable level of image quality for equivalent breast thicknesses of up to 90mm. For higher equivalent breast thicknesses, the SDNRs were below the achievable level but above the minimum.

## 4.2 Local dense area

The local dense area test showed that the AEC identifies the presence of the dense area and increases the mAs in order to maintain SNR. As expected, the auto mean AEC mode did not respond as much to the local dense area as the auto sensor mode and this resulted in a slightly steeper drop in SNR. The positioning of the aluminium relative to the super-pixels will affect the exposure level.

The AEC essentially operates in the same manner as the 3Dimensions. The system can respond to changes in density by adjusting the mAs. If the calculated exposure time exceeds a certain limit for the given exposure, then it will increase the kV, which will generally be for denser breasts or if the output of the x-ray tube is low. The tube potential is selected almost entirely on the displayed compressed breast thickness. The system AEC does not automatically recognise implants, so a manual AEC sensor position is required or manually set exposures are required.

## 4.3 Noise analysis

Noise analysis showed that quantum noise dominates the noise over the whole range of incident air kermas measured (19 to 460µGy) (Figure 10). The results show that there are minimal contributions from electronic noise and that structural noise contributes less than

20% of the total variance across the full air kerma range and less than 10% at more clinically relevant levels.

## 4.4 Image quality

Threshold gold thicknesses for a range of detail diameters are shown in Figure 11. At an MGD of 1.76mGy (close to that selected for the equivalent thickness of PMMA in Standard mode), the image quality was better than the achievable level for all contrast detail diameters.

Threshold gold thickness measurements at different dose levels for the 0.1mm and 0.25mm diameter details were used to calculate Dance MGDs to a 60mm equivalent breast required for the minimum and achievable levels of image quality (Figure 12). The results are slightly poorer than for the technical evaluation of the 3Dimensions [1]; Hologic have stated that this may be due to normal system to system variation.

## 4.5 Quantitative measurements

The quantitative measurements, as indicated by MTF, NNPS and DQE curves (Figures 13, 14 and 15), were provided for reference. The MTF associated with the detector is expected to be the same in the two directions. The low frequency component of the MTF was lower in the lateral direction compared to the CWE to nipple direction. This is due to extra focal radiation due to a change in the design of the near collimator to compensate for the moving focal spot used in tomosynthesis imaging. This may have a slight adverse effect on image quality.

There is a spike in the NNPS, however it is not expected to affect the clinical images. The system is flat fielded with a block of PMMA covering the whole detector with the anti-scatter grid present. Hologic states that the spike in the NNPS is associated with the anti-scatter grid during the flat fielding. The NNPS spike can be present in images acquired both with and without the grid in the beam. Repeated measurements showed variations in the magnitude of the spike with a general increasing trend throughout the evaluation period. No correlations were seen with exposure time, x-ray tube current, or detector dose indicator (DDI). If a flat field correction is undertaken without the anti-scatter grid present, then a spike in the NNPS would not be expected in these results.

The DQE as defined by the IEC [21] is for the detector alone. These measurements were made within the system and the calculated DQE was affected by the system effects on the MTF and NNPS.

### 4.6 Other tests

The miscellaneous results presented under the section “Other tests” were satisfactory.

## 5. Conclusions

The technical performance of the Hologic Envision in 2D mode was found to be satisfactory.

The Dance MGD to the 53mm thick standard breast in 2D mode was found to be 1.36mGy for the normal dose AEC mode. This is well below the remedial level. The image quality, as measured by threshold gold thickness, is better than the achievable level.

## 6. Acknowledgements

The authors (John Loveland and Alistair Mackenzie) would like to acknowledge the help of Hologic staff in providing access to the equipment and for technical support. We also thank Hologic for covering the travel, accommodation and meal costs during our visit.

## References

[1] A. Mackenzie and J. Oduko, “NHS Breast Screening Programme Equipment Report Technical Evaluation of Hologic 3Dimensions digital mammography system in 2D mode,” Public Health England, London, 2019.

[2] Public Health England, “NHS Breast Screening Programme Equipment Report: Technical evaluation of GE Senographe Pristina digital mammography system in 2D mode,” Public Health England, London, 2019.

[3] C. Strudley, A. Hadjipanteli, J. Oduko and K. Young, “NHS Breast Screening Programme Equipment Report: Technical evaluation of Fujifilm AMULET Innovality digital breast tomosynthesis system,” Public Health England, London, 2018.

[4] N. Tyler, K. Young, J. Oduko and A. Mackenzie, “NHS Breast Screening Programme Equipment Report: Technical Evaluation of IMS Giotto Class digital mammography system in 2D mode,” Public Health England, London, 2019.

[5] J. Loveland and A. Mackenzie, “NHS Breast Screening Programme Equipment Report: Technical Evaluation of Siemens MAMMOMAT B.brilliant digital mammography system in 2D mode,” NHS England, Leeds, 2024.

[6] E. Kulama, A. Burch, I. Castellano, C. Lawinski, N. Marshall and K. Young, “NHSBSP Equipment Report 0604: Commissioning and routine testing of full field digital mammogaphy systems,” NHS Cancer Screening Programmes, Sheffield, 2009.

[7] R. van Engen, S. van Woudenberg, H. Bosmans, K. Young and M. Thijssen, “European guidelines for quality assurance in breast cancer screening and diagnosis (4th edition): European protocol for the quality control of physical and technical aspects of mammgography screening,” European Commission, Luxembourg, 2006.

[8] E. Perry, M. Broeders, C. de Wolf, S. H. R. Törnberg and L. von Karsa, “European guidelines for quality assurance in breast cancer screening and diagnosis - Fourth eddition Supplements,” European Commission, Luxembourg, 2013.

[9] A. C. Moore, D. R. Dance, D. S. Evans, C. P. Lawinski, E. M. Pitcher and A. Rust, “The commissioning and routine testing of mammographic X-ray systems,” Institute of Physics and Engineering in Medicine, York, 2005.

[10] D. R. Dance, “Monte Carlo calculation of conversion factors for the estimation of mean glandular breast dose,” *Physics in Medicine and Biology,* vol. 35, pp. 1211-19, 1990.

[11] D. R. Dance, C. L. Skinner, K. C. Young, J. R. Beckett and J. C. Kotre, “Additional factors for the estimation of mean glandular breast dose using the UK mammography dosimetry protocol,” *Physics in Medicine and Biology,* vol. 45, pp. 3225-40, 2000.

[12] D. R. Dance, K. C. Young and R. E. van Engen, “Further factors for the estimation of mean glandular dose using the United Kingdom, European and IAEA dosimetry protocols,” *Physics in Medicine and Biology,* vol. 54, pp. 4361-72, 2009.

[13] I. Sechopoulos, D. R. Dance, J. M. Boone, H. T. Bosmans, M. Caballo, O. Diaz, R. van Engen, C. Fedon, S. J. Glick, A. M. Hernandez, M. L. Hill, K. W. Hulme, R. Longo, C. Rabin and W. B. Sanderink, “Joint AAPM Task Group 282/EFOMP Working Group Report: Breast dosimetry for standard and contrast-enhanced mammography and breast tomosynthesis,” *Medical Physics,* vol. 51, no. 2, pp. 712-739, 2023.

[14] A. Alsager, K. C. Young and J. M. Oduko, “Impact of heel effect and ROI size on the determination of contrast-to-noise ratio for digital mammography systems,” *International Society for Optics and Photonics, Proc. SPIE 6913 Medical Imaging 2008: Physics of Medical Imaging,* 2008.

[15] A. Hernandez, A. Seibert, A. Nosratieh and J. Boone, “Generation and analysis of clinically relevant breast imaging x-ray spectra,” *Medical Physics,* vol. 44, no. 6, p. 148–2160, 2017.

[16] M. Berger, J. Hubbell, S. Seltzer, J. Chang, J. Coursey, R. Sukumar, D. Zucker and K. Olsen, “XCOM: Photon Cross Sections Database (version 1.5),” November 2010. [Online]. Available: https://www.nist.gov/pml/xcom-photon-cross-sections-database.

[17] R. van Engen, S. Schopphoven, K. Pedersen, N. Marshall, A. Mackenzie, P. Heid, P. Golinelli, M. Chevalier and P. Baldelli, “Quality Control in Digital Breast Tomosynthesis (DBT): EFOMP Protocol 02.2024,” European Federation of Organisations for Medical Physics, Utrecht, 2024.

[18] K. Young, J. Oduko, H. Bosmans, K. Nijs and L. Martinez, “Optimal beam quality selection in digital mammography,” *British Journal of Radiology,* vol. 79, pp. 981-990, 2006.

[19] K. Young, J. Cook and J. Oduko, “Automated and human determination of threshold contrast for digital mammography systems,” *In Proceedings of the 8th International Workshop on Digital Mammography, Berlin: Springer-Verlag,* pp. 4046: 266-272, 2006.

[20] K. Young, A. Alsager, J. Oduko, H. Bosmans, B. Verbrugge, T. Geertse and R. van Engen, “Evaluation of software for reading images of the CDMAM test object to assess digital mammography systems,” *Medical Imaging 2008: Physics of Medical Imaging, Proceedings of the SPIE, Volume 6913, article id. 69131C,,* 2008.

[21] International Electrotechnical Commission, “IEC 62220-1-2: Determination of the detective quantum efficiency – Detectors used in mammography,” International Electrotechnical Commission, Geneva, 2007.

[22] International Electrotechnical Commission, “IEC 60336:2020 - Medical electrical equipment - X-ray tube assemblies for medical diagnosis - Focal spot dimensions and related characteristics,” International Electrotechnical Commission, Geneva, 2020.